Applied Catalysis B: Environmental 303 (2022) 120887

Contents lists available at ScienceDirect

Applied Catalysis B: Environmental

journal homepage: www.elsevier.com/locate/apcatb

Engineering interfacial charge transfer channel for efficient photocatalytic H_2 evolution: The interplay of CoP_x and Ca^{2+} dopant

Xiaohui Ren [a,b], Fei Liu [c], Qi Wang [a,b], Hui Song [b], Shunqin Luo [a,b], Sijie Li [a,b], Gaoliang Yang [a,b], Bowen Deng [a,b], Zongyu Huang [c], Xu-Sheng Wang [b,e], Li Shi [d,*], Jinhua Ye [a,b,f,**]

[a] Graduate School of Chemical Sciences and Engineering, Hokkaido University, Sapporo 060-0814, Japan
[b] International Center for Materials Nanoarchitectonics (WPI-MANA), National Institute for Materials Science (NIMS), 1-1 Namiki, Tsukuba, Ibaraki 305-0044, Japan
[c] School of Physics and Optoelectronic, Hunan Key Laboratory for Micro-Nano Energy Materials and Devices, Xiangtan University, Hunan 411105, PR China
[d] School of Materials Science & Chemical Engineering, Ningbo University, Ningbo, Zhejiang 315211, PR China
[e] School of Materials Science and Engineering, Zhejiang Sci-Tech University, Hangzhou 310018, PR China
[f] TJU-NIMS International Collaboration Laboratory, School of Material Science and Engineering, Tianjin University, Tianjin 300072, PR China

ARTICLE INFO

Keywords:
CdS
Interfacial engineering
Ultrafine CoP_x nanoparticles
Photocatalytic H_2 generation

ABSTRACT

Cobalt phosphide (CoP_x) has been developed as a cost-effective cocatalyst for photocatalytic H_2 evolution with the advantages of excellent conductivity, strong reduction ability, good thermal and chemical stability. In this work, a facile preparation strategy was proposed to fabricate ultrafine CoP_x nanoparticles on the surface of CdS. The effective H_2 production over ultrafine CoP_x nanoparticles has been realized. In addition, we found Ca^{2+} as an alkaline earth metal ion can promote the interaction between CdS and CoP_x. Both experimental results and density function theory indicate that the Ca^{2+} dopant can act as surface trapping sites on CdS and lead to efficient separation of photogenerated electron-hole pairs. The integration of CoP_x and Ca^{2+} dopant can synergistically enhance both photogenerated electron-hole separation as well as interfacial charge transfer, which enables a remarkable improvement on the H_2 generation performance of CdS. The photocatalytic H_2 generation rate of Ca-modified CoP_x@CdS can reach up to 2441.5 μmol h^{-1} under optimal conditions with the apparent quantum efficiency as high as 35.4% at 420 nm. This finding motivates the development of simplified fabrication procedures for constructing and modifying cobalt active sites with efficient photocatalytic H_2 generation performance.

1. Introduction

Hydrogen (H_2) is known as a clean and sustainable energy carrier that plays an essential role in the low-carbon economic system. In the past decades, the developments of hydrogen energy system as well as applications of hydrogen in different fields have attracted worldwide interests [1–5]. Until now, a variety of photocatalysts have been exploited in the H_2 evolution reaction. However, semiconductor-based photocatalysts usually suffer from rapid electron-hole recombination, lack of reaction sites, and low efficiency in solar to chemical energy conversion. To overcome the aforementioned difficulties, a cocatalyst is usually required to enhance the separation of photogenerated electron-hole pair and to provide sufficient active sites for surface chemical reactions [6–13]. Generally, most highly efficient photocatalytic systems are realized by utilizing noble-metal-based cocatalysts such as Pt, Pd, Ag, etc [14]. Unfortunately, noble metals are too scarce and expensive to be used for large-scale energy production. Therefore, the exploration and development of cost-effective cocatalysts are highly desired.

Of particular interest, cobalt-based transition metal phosphides have attracted worldwide attention as promising noble metal-free alternatives for noble-metal-based cocatalysts in photocatalytic H_2 production [15]. Amongst various cobalt-based materials, cobalt phosphides (CoP_x) including Co_2P, CoP, CoP_2, CoP_3, etc. have become the hot topic in catalytic H_2 production owing to the metal-like characteristics of Co–P bond [16–21]. With lower Fermi energy level, it was anticipated that CoP_x can play a significant role in promoting both electrocatalytic and photocatalytic H_2 evolution [22]. Previous studies indicated that

* Corresponding author.
** Corresponding author at: Graduate School of Chemical Sciences and Engineering, Hokkaido University, Sapporo 060-0814, Japan
E-mail addresses: shili1@nbu.edu.cn (L. Shi), Jinhua.YE@nims.go.jp (J. Ye).

https://doi.org/10.1016/j.apcatb.2021.120887
Received 16 September 2021; Received in revised form 29 October 2021; Accepted 31 October 2021
Available online 4 November 2021

rational construction of Schottky junction between CoP_x and semiconductor CdS could enable promising improvements on photocatalytic H_2 evolution performance [23–27]. Meanwhile, the efficient electron transfer property endows photogenerated electrons with great capability for reducing adsorbed H^+ into H_2.

Moreover, it has been reported that metal cations can be employed to tailor the electronic structure of CdS for further enhancing the photocatalytic performance [28]. By doping with a donor impurity, the impurity levels below the conduction band may induce the generation of electron trap sites on the surface of CdS, which is believed to hinder photogenerated electron-hole recombination and increase the lifetime of photogenerated electrons [29–32]. Common alkaline-earth metal ions (such as Mg^{2+}, Ca^{2+}, Sr^{2+}, Ba^{2+}) with good stability and charge transition properties have been applied for modifying semiconductor [33]. Benefitted from the good electron-donating feature and stability of alkaline-earth metal ions, significant enhancement on the photocatalytic activities have been realized after doping with alkaline-earth metal ions [34]. However, it has rarely been applied in modifying CdS-based photocatalysts.

Herein, we proposed a convenient preparation strategy to fabricate ultrafine CoP_x nanoparticles and applied it into photocatalytic H_2 evolution. By utilizing organophosphorus compound triphenylphosphine (PPh_3) as phosphorous source, the as-fabricated CoP_x nanoparticles are intrinsically encapsulated by carbon layer and applied as the cocatalyst for photocatalytic H_2 evolution. To our notice, this is the first report about the design of carbon assisted CoP_x@CdS interfacial structure through the assistance of PPh_3, which does not require additional hybrid carbon source via multi-step reactions. The relation between metal dopants and the catalytic performance has been investigated. Benefitted from the interfacial engineering, the charge transfer behavior between CdS and CoP_x has been modified through Ca^{2+} dopant. Specially, the photocatalytic H_2 generation over Ca-modified CoP_x@CdS can reach up to 2441.5 μmol h^{-1} with the apparent quantum efficiency of 35.4% at 420 nm. Finally, the mechanism was explored to reveal the effect of Ca^{2+} dopant on the underlying mechanism of the excellent photocatalytic H_2 generation performance.

2. Experimental section

2.1. Fabrication of CoP_x@CdS

In order to prepare CoP_x@CdS, a certain amount of PPh_3 was first mixing and grinding with commercial CdS. After the self-assembling process of PPh_3 molecules, $CoCl_2$ with mole ratio of 0.5% were added and annealed at 300–600 °C under argon atmosphere.

2.2. Fabrication of Ca-modified CoP_x@CdS

In detail, the commercial CdS was first mixed with 0.5% mole proportions of Co^{2+} and Ca^{2+} in ethanol solution. After that, the dried mixture was annealed at temperatures at 500 °C under argon atmosphere. The resulting sample was denoted as Ca-modified CoP_x@CdS and applied as photocatalyst for hydrogen generation. For comparison, Ca-modified CdS and CdS-P were prepared by respectively annealing the mixture of CdS/$CaCl_2$ and CdS/PPh_3 under same conditions. The annealing CdS refers to the CdS annealed directly at temperatures at 500 °C under argon atmosphere without any other modification. In addition to Ca^{2+}, CdS has been modified with other metals dopants (Mg^{2+}, Sr^{2+}, Ba^{2+}, Cr^{3+}, Al^{3+}, V^{3+}, Nd^{3+}, and Mo^{5+}) in equal amounts.

2.3. Photocatalytic H_2 evolution activity

Photocatalytic H_2 evolution activities were evaluated under visible-light irradiation. A 300 W xenon arc lamp equipped with a 420 nm cut-off filter was applied as the light source. In all experiments, 260 mL of 0.25 M/0.35 M Na_2S/Na_2SO_3 solution was taken as sacrificial reductant, and 100 mg of as-prepared sample was used as photocatalyst for achieving H_2 half reaction. The amount of produced H_2 was recorded and analyzed by an online gas chromatograph (GC-8A, Shimadzu Corp., Ar carrier, TCD, Japan) with argon as the carrier gas.

3. Results and discussion

3.1. Fabrication CoP_x@CdS for photocatalytic H_2 production

The detail synthetic routes of CoP_x@CdS photocatalyst have been demonstrated in Fig. 1a. Different from previous reported phosphatizing protocols for synthesize CoP_x-based hybrids, our synthetic strategy based on the organophosphorus compound PPh_3 does not require flammable compounds (e.g. PH_3 or H_2, etc.) or corrosive conditions, which makes it much safer and easier to manipulate comparing to conventional methods [35–37]. Microstructural characterizations including transmission electron microscopy (TEM), high-resolution TEM (HRTEM) and energy dispersive X-ray spectroscopy (EDX) were utilized to unveil the morphology of CoP_x@CdS structure. As shown in Fig. 1b–e, the amorphous carbon can be observed on the surface of CdS after annealing, where ultrafine CoP_x nanoparticles are separately anchored in the amorphous carbon cages. The elemental mapping displays that C and Co elements uniformly distribute on the surface of CdS, while P element concentrates at interface region between CdS and carbon cages (Fig. S1). In this situation, the amorphous carbon cages act as the substrate for the growth of Co active sites (Fig. S2). The light absorption properties are demonstrated in Fig. 1f, and an increment on light absorption properties over the visible wavelength range has been discovered benefitted from the incorporation of CoP_x [38]. The nanostructure of CdS and CoP_x@CdS has been analyzed by Raman spectroscopy. As shown in Fig. 1g, the first and second longitudinal optical phonon modes (1LO and 2LO) of CdS can be observed [39]. However, the characteristic peaks of CoP_x (262.7 cm^{-1}) cannot be identified due to its low amount when the peak is overlapping with that of CdS [40–42]. Meanwhile, the weak D and G band vibrations of carbon in Fig. S3 suggest that amorphous carbon has been formed [43–45]. Fig. 1h demonstrates the photocatalytic H_2 evolution activities of CoP_x@CdS prepared under calcination temperatures varying from 300 °C to 600 °C. The highest H_2 evolution rate of 1425.2 μmol h^{-1} has been realized under the optimized temperature of 500 °C, which indicate the formation of ultrafine CoP_x nanoparticles as well as interfacial interaction between CdS and CoP_x is optimized in this condition as we previously reported [46].

3.2. Synthesis and characterization of Ca-modified CoP_x@CdS

It was known that the long distance between CdS and Co active sites would lead to negative effect on electron transport and insufficient active sites, which is undesirable for photocatalytic reactions. By taking Ca^{2+} dopant to initiate interfacial engineering and to modifying the interface between CdS and CoP_x, the carbon layer would be tightly wrapped on CdS surface (Fig. 2a). It can be regarded that an intimate interfacial contact between CdS and CoP_x has been achieved after Ca^{2+} modification, which may be attributed to ascending reducibility of Ca-modified CdS together with strong interaction between PPh_3 and Ca^{2+} dopant [47]. HRTEM images in Fig. 2b depict that the ultrafine CoP_x nanoparticles are wrapped by thin amorphous carbon layer and anchored on the surface of CdS (the dark/light contrasts observed along radial direction indicate the thickness is approximately 4 nm, Fig. S4). The intimate interfacial contact between CdS and CoP_x may support fast charge transfer with more accessible active sites. The SAED of CdS can be observed in Fig. 2c, which indicates the typical single crystal structure of CdS [48]. The inter-planar spacing≈ 0.242 nm is corresponding to the (102) plane of hexagonal CdS, while the d-spacing of 0.28 nm is ascribed to the (002) plane of CoP_x (Fig. 2d). Besides that, EDX mappings (Fig. 2e and Fig. S5) also indicate the uniformly distribution of C, Co, P, and Ca elements on CdS. The chemical compositions of the

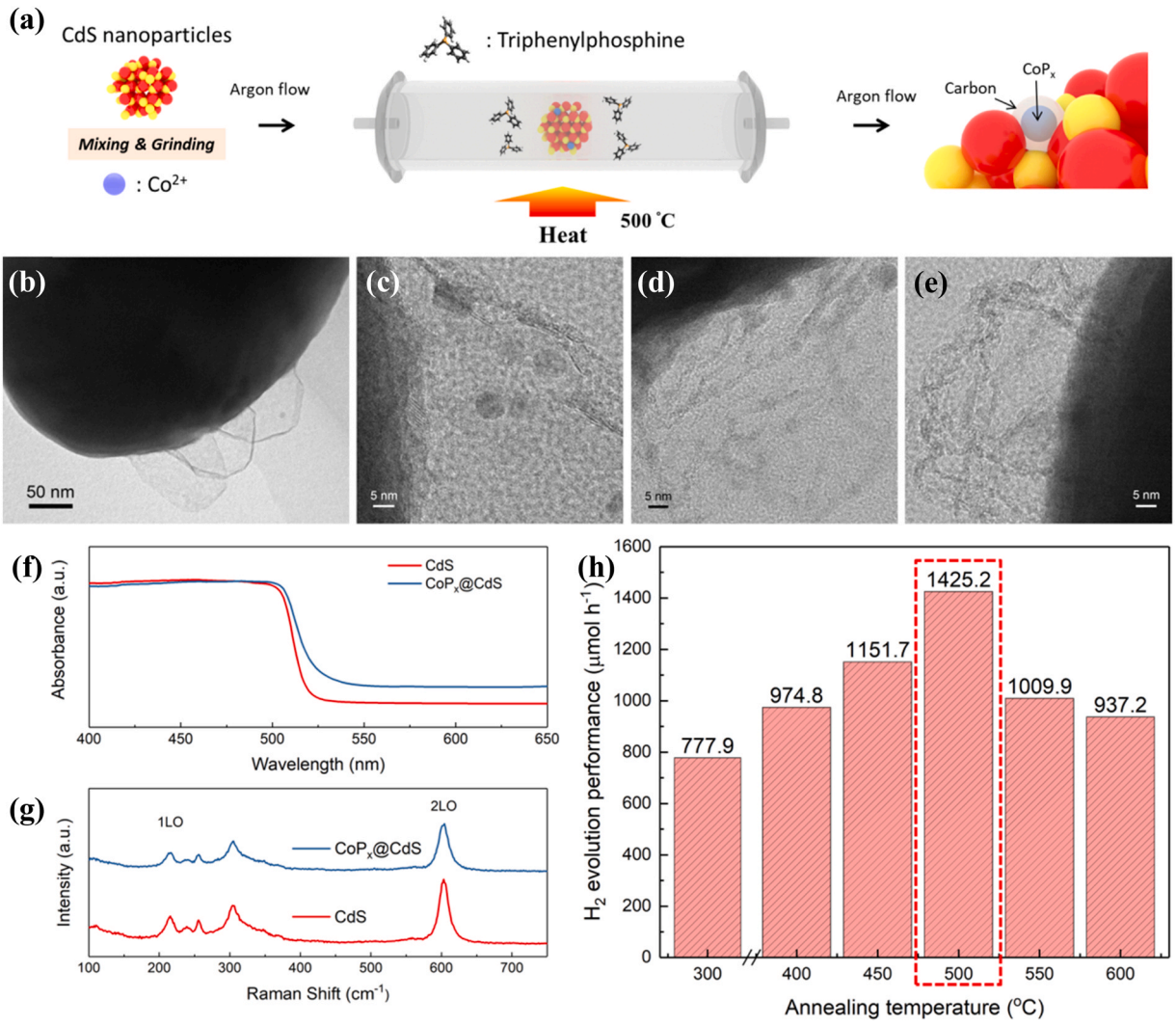

Fig. 1. (a) Schematical illustration on the synthesize processes of CoP_x@CdS. (b)-(e) TEM images of CoP_x@CdS. (f) Light absorption spectra and (g) Raman spectra of CdS and Ca-modified CoP_x@CdS. (h) The H_2 evolution performance of CoP_x@CdS annealed under 300–600 °C. (The optimal annealing temperature has been marked in dashed border).

samples (Table S1) were quantitatively determined using inductively coupled plasma-optical emission spectrometry (ICP-OES), and the mass ratio of Ca has been determined to be 0.1 wt%.

X-ray diffraction (XRD) measurements were conducted to investigate the structure of the Ca-modified CoP_x@CdS and related samples (Fig. 3a). The XRD results of CdS and Ca-modified CoP_x@CdS after calcination under 500 °C show no distinct difference, and the patterns can be indexed into hexagonal CdS (P63mc space group, JCPDS No. 06-0314), the peaks at 24.9°, 26.6°, 28.2° are corresponding to (100), (002), and (101) planes of wurtzite CdS, respectively. No obvious shift of the XRD peaks can be observed since the ionic radius of Ca^{2+} (0.099 nm) is similar to that of Cd^{2+} (0.097 nm) (Fig. S6) [49]. Besides, the optical absorption spectra demonstrate the slightly decreased bandgap of Ca-modified CdS comparing to annealed CdS (Fig. S7). In addition, we have conducted X-ray photoelectron spectroscopy (XPS) to study the characteristics of Ca-modified CoP_x@CdS. Full-survey spectrum shows the existence of Cd, S, C, O, Co, P, and Ca elements in the hybrid (Fig. S8). Meanwhile, the peak centered at 347.3 eV corresponds to $Ca2p_{3/2}$ indicating that calcium mainly exists as Ca^{2+}. In the high-resolution spectrum of Co 2p (Fig. 3b), the binding energy of 779.6 eV is very close to that of Co $2p_{3/2}$ in CoP_x, which suggests a new electron transfer channel Co-P formed due to interaction between Co and P as previously reported [29,50,51]. Other peaks belong to the Co $2p_{1/2}$ and Co $2p_{3/2}$ of Co^{2+} components can be attributed into unavoidable surface oxidation. Comparing to the results of EDX (Fig. S9) and ICP-OES, the atomic percentage of Ca^{2+} is much higher when analyzed by XPS (Table S2). Therefore, it can be expected that most of Ca^{2+} ions are existed mainly on the surface of CdS.

The electron transfer process has been elucidated by photoluminescence and time-resolved photoluminescence spectra under room-temperature. In our experiments, a sharp emission band centered at 520 nm and a broad emission band centered at 650 nm can be observed (Fig. 4a) when the photocatalysts were excited at a wavelength of 420 nm. The two characteristic peaks can be assigned to band-to-band transition and surface radiative transition resulting from band-gap emission and trap-state emission, respectively. After Ca doping, the band-gap emission of CdS is dramatically quenched which indicates a low recombination rate of carriers. In contrast, the trap-state emission becomes stronger and broader after Ca doping, this phenomenon reveals that photon-induced carriers can be extracted out to reach the electron trapping sites centered on the surface owing to the increase of Ca-related defects located on the surface [33]. We also notice that both band-gap emission and trap-state emission were remarkably quenched upon the loading of CoP_x. This photoluminescence quench behavior indicates fast charge transfer of electrons from CdS to CoP_x, attributing to higher electron-hole separation ability in Ca-modified CoP_x@CdS than that in

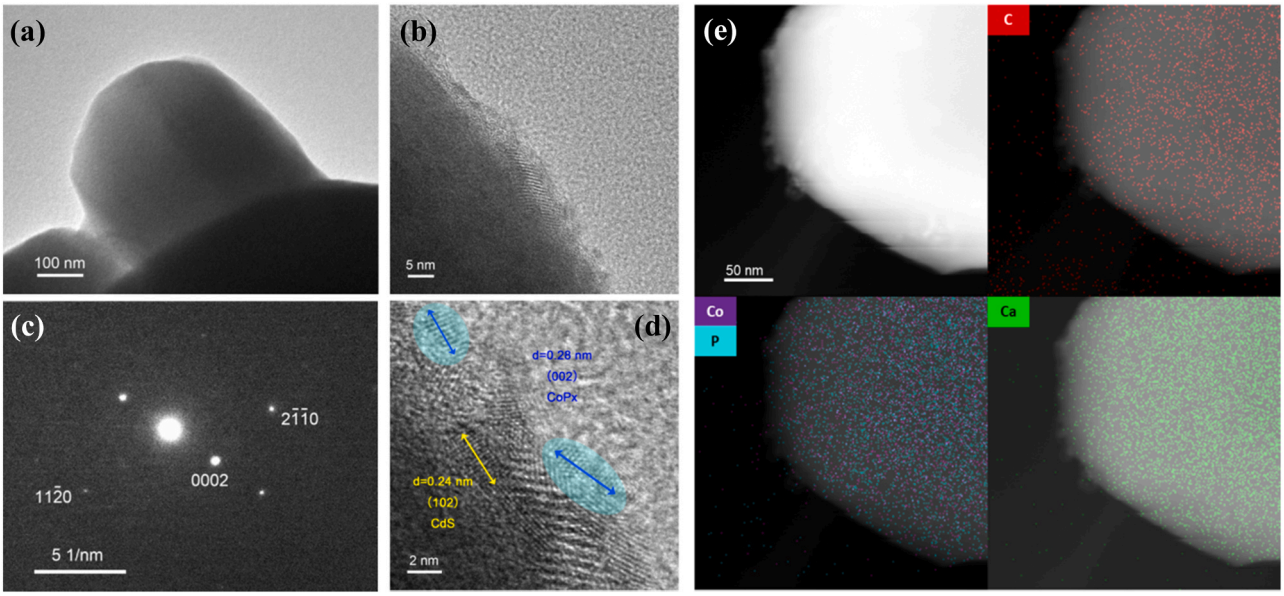

Fig. 2. (a) TEM image, (b) HRTEM image and (c) SAED pattern of Ca-modified CoPx@CdS. (d) HRTEM image on the interface between carbon, CoP_x and CdS. (e) HAADF and overlapping EDX mappings of C, Co, P, and C elements on the Ca-modified CoP_x@CdS.

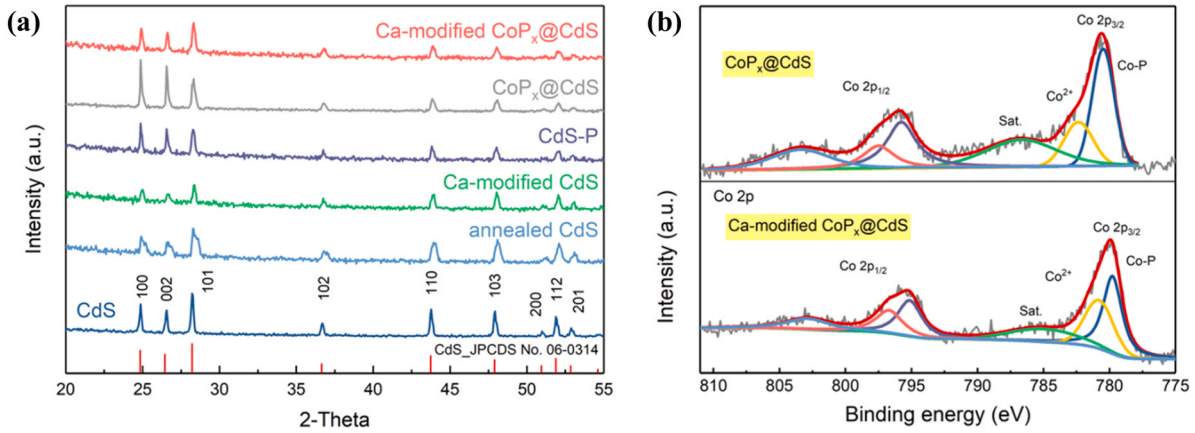

Fig. 3. (a) XRD analysis of CdS, annealed CdS, Ca-modified CdS, CdS-P, CoP_x@CdS, and Ca-modified CoP_x@CdS. (b) High-resolution XPS spectra of Co 2p for CoP_x@CdS and Ca-modified CoP_x@CdS.

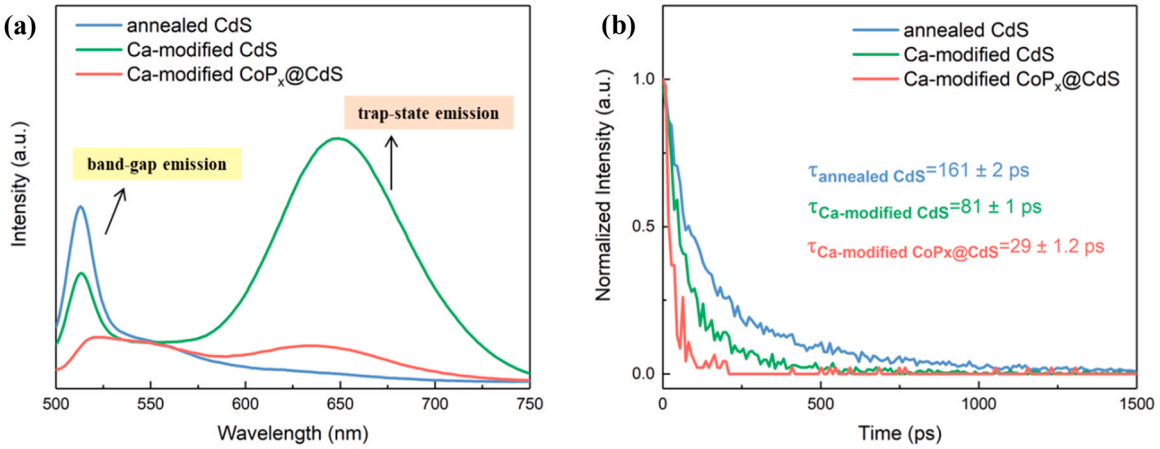

Fig. 4. Charge transfer dynamics analyzed by (a) Steady-state photoluminescence spectra and (b) Time-resolved photoluminescence spectra of annealed CdS, Ca-modified CdS, and Ca-modified CoP_x@CdS. (excitation is 420 nm).

pure CdS.

In order to gain in-depth understanding on the transfer dynamics of photogenerated electron in the conduction band of CdS, we have investigated the time-resolved photoluminescence spectra over obtained systems together with the average lifetime of excitons. The charge-transfer dynamics between CdS before and after heat treatment has been studied at first. As shown in Fig. S10, the decay time for CdS (band-gap emission, monitored at 520 nm) has been greatly prolonged from 72 ± 0.7 ps to 161 ± 2 ps after annealing process. This phenomenon can be explained as the photogenerated electrons are surprisingly long lived in the presence of effective trapping states, and endowed with the capability to reach the surface for redox reaction in consequence [30, 52]. In addition, a much shorter carrier lifetime of Ca-modified CdS (τ = 81 ± 1 ps) compared to annealed CdS (τ = 161 ± 2 ps) may indicate that Ca dopant is likely to trigger efficient electron extraction from CdS to defect sites (Fig. 4b). Besides that, a dominant time constant has been achieved by CoP_x@CdS (τ = 37 ± 1.5 ps), which features smooth carrier transfer channel with intimate interfacial contact between CdS and CoP_x active species (Fig. S11). The acceleration of decay kinetics for Ca-modified CoP_x@CdS further decreases the lifetime from 37 ± 1.5 ps to 29 ± 1.2 ps (Fig. S12). It is believed that fast charge injection from CdS to CoP_x active sites has been realized after Ca^{2+} modification. In this regards, the Ca^{2+} would act as the interfacial mediator for accelerating the electron transfer, attributing to effective electron-hole separation.

3.3. Photocatalytic H_2 generation performance over Ca-modified CoP_x@CdS

The photocatalytic H_2 evolution performance of as-prepared samples was evaluated under visible light (λ > 420 nm) illumination. In detail, CdS alone can only demonstrate a poor H_2 production rate of 284.5 μmol h^{-1} (Fig. S13). After annealing, the H_2 production efficiency can be promoted to 639.0 μmol h^{-1} (Fig. 5a). Compared with CdS-P (937.2 μmol h^{-1}) and CoP_x@CdS (1425.2 μmol h^{-1}), the photocatalytic H_2 generation rate of Ca-modified CoP_x@CdS has reached the highest value of 2441.5 μmol h^{-1}, with turnover frequency (TOF) as high as 703.2 h^{-1} [53]. The H_2 production performance indicates the obvious enhancement on hydrogen evolution activity of CdS is depending on the interaction between Ca^{2+} and carbon as we have explained in our previous works [46, 54–56]. The advantages of Ca^{2+} for improving the H_2 generation activity over CoP_x@CdS have been verified through a comprehensive overview on the photocatalytic H_2 generation performance of CoP_x@CdS that modified by other alkaline-earth metal ions (Mg^{2+}, Sr^{2+}, Ba^{2+}) or aliovalent metal ions (such as Cr^{3+}, Al^{3+}, V^{3+}, Nd^{3+}, and Mo^{5+}) as demonstrated in Fig. 5b. The enhancements on H_2 production performance follow in the order of Ca>Mo>Ba>Mg>Nd>Sr>Al>V>Cr. The results suggest that alkaline-earth metal ions (Mg^{2+}, Ca^{2+}, Sr^{2+}, Ba^{2+}) play positive roles in modifying CdS for promoting photocatalytic H_2 production.

The apparent quantum efficiency (AQE) and stability measurement of the optimal Ca-modified CoP_x@CdS has been provided. The curve of AQE (Fig. 5c) of Ca-modified CoP_x@CdS is dependent on the light wavelength which is related to the optical absorbance of the photocatalyst. The performance of Ca-modified CoP_x@CdS can reach up to 35.4% at 420 nm and is comparable or even higher than that of previous reported CdS-based photocatalyst systems (Table S3 and Table S4). The cycling stability over Ca-modified CoP_x@CdS has been investigated as shown in Fig. 5d. Notably, our photocatalyst exhibits outstanding

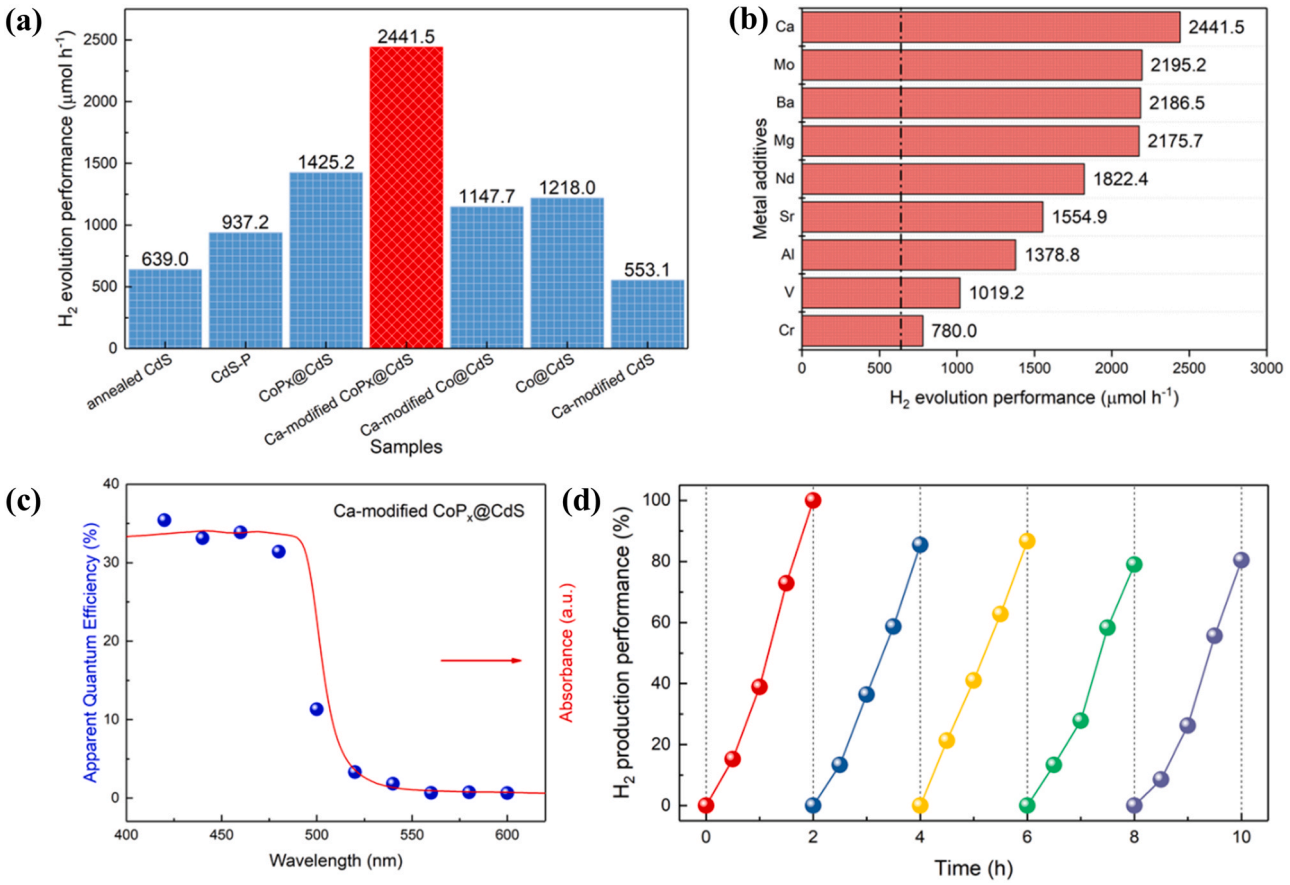

Fig. 5. (a) Comparison on the photocatalytic H_2 evolution performance between annealed CdS, CdS-P, CoP_x@CdS, Ca-modified CoP_x@CdS, Ca-modified Co@CdS, Co@CdS and Ca-modified CdS. (b) The photocatalytic H_2 evolution performance of CoP_x@CdS modified by different metal dopants. (The dash-dot line represents pristine H_2 generation performance of annealed CdS). (c) AQE curve of Ca-modified CoP_x@CdS. (d) Cycling stability measurement over Ca-modified CoP_x@CdS.

stability in Na_2S/Na_2SO_3 solution, and the H_2 evolution performance can retain after five cycling tests without significant decrease. Moreover, the H_2 production of Ca-modified CoP_x@CdS depicts linear increasing without apparent decay (Fig. S14), sustaining for 24 h under appropriate conditions (20 mg Ca-modified CoP_x@CdS photocatalyst, dispersed into 260 mL of 0.25/0.35 Na_2S/Na_2SO_3 solution, irradiated by 420 nm monochromatic light). A total amount of 289 μmol H_2 has been produced with a steady rate of 12 μmol h^{-1} during the course of long-term stability test for 24 h. All these results prove that Ca-modified CoP_x@CdS is a robust H_2 production photocatalyst.

3.4. DFT calculation and mechanism analysis

The DFT calculation has been carried out to gain in-depth understanding on the intrinsic properties of Ca-modified CoP_x@CdS and underlying H_2 generation mechanism [46]. First of all, the Gibbs free energy change for H* adsorption (ΔG_{H^*}) values of CoP_x@CdS before and after Ca^{2+} modification have been investigated. As shown in Fig. 6a, the obtained ΔG_{H^*} of pristine CoP_x@CdS is 0.17 eV, while the ΔG_{H^*} of the system decreases to −0.06 eV when a Cd atom in CdS is replaced by Ca atom. It can be found that Ca^{2+} modification can greatly reduce the $|\Delta G_{H^*}|$ of CoP_x@CdS, which signifies Ca-modified CoP_x@CdS is kinetic favorable for the adsorption and desorption of hydrogen comparing to that of CoP_x@CdS. In addition, the charge transferring behavior has been elucidated by analyzing the charge density difference. The charge densities are redistributed at the hetero-interface between CdS and CoP_x layer after Ca^{2+} doping as shown in Fig. S15, which suggest much more favorable charge transfer between CdS and CoP_x and accumulation of charge on the interface owing to the existence of Ca^{2+} dopant. Moreover, the electron density accumulation and depletion will result in the formation of the built-in electric field between the adjacent CdS and CoP_x layer (Fig. S16 and Table S5).

Similarly, the electron localization functions (Fig. 6b) show that the electron locality of the Co and Cd atoms is weak, while that of the P, S and Ca atoms is strong. This fact can be attributed to that Co can inject electrons into the P atoms and Ca dopants, and Ca^{2+} dopants are bridging the interfacial electronic structure as well as charge transfer between CdS and CoP_x. In addition, the total density of states (TDOS) of CoP_x@CdS before and after Ca^{2+} doping have been performed in Fig. S17, pronounced peak changes can be observed in the close vicinity of Fermi level when comparing the DOS between CoP_x@CdS and Ca-modified CoP_x@CdS systems. The results indicate that electron density near the Fermi level becomes more localized, and an enhancement of local electrical conductivity can be realized owing to the dopant effect of Ca. Meanwhile, to further clarify the effect of Ca doping on the electronic structure, the partial density of states (PDOS) for the orbitals of Cd atoms, Co atoms and Ca atom are shown in Fig. S18. The overlapping of Cd, Co, and Ca orbitals suggest the formation of electron transport channels between Co and Ca which may be the results from orbital hybridization [57,58]. In this regards, photo-excited electrons are first captured in surface defect sites of Ca-modified CdS. Then, the trapped charge carriers would further transfer to CoP_x nanoparticles more easily through the interface of heterostructure due to the lower Fermi level of CoP_x as compared to CdS, and subsequently participate into

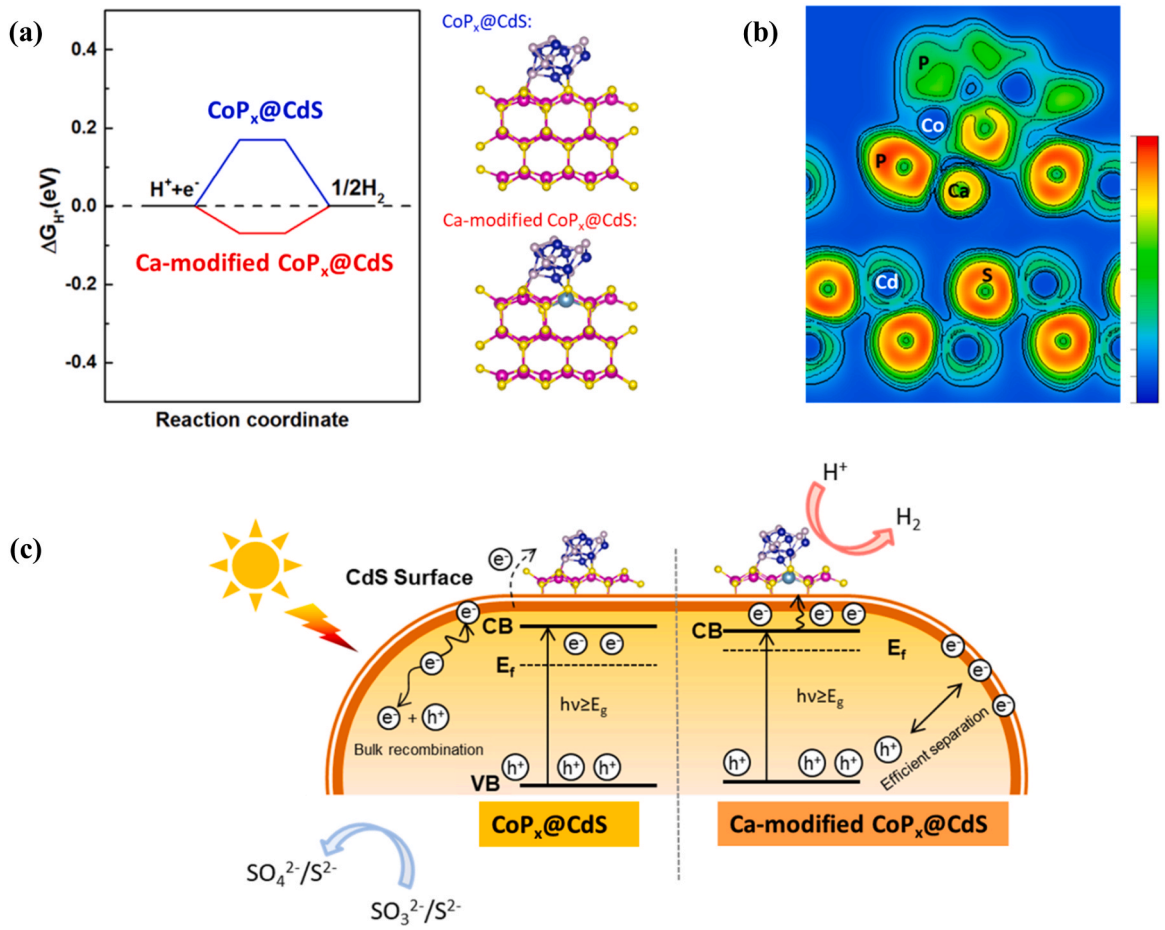

Fig. 6. (a) The calculated Gibbs free energy of H adsorbed CoP_x@CdS and Ca-modified CoP_x@CdS and corresponding atomic structure. (Yellow balls: Sulfur atoms; Magenta balls: Cadmium atoms; Gray balls: Phosphorus atoms; Blue balls: Cobalt atoms; Wathet balls: Calcium atoms) (b) The side views of the electron localization functions from the (010) section of the Ca-modified CoP_x@CdS. The concentration of electrons increases from blue to red. (c) Mechanism illustration on charge migration in Ca-modified CoP_x@CdS. (For interpretation of the references to colour in this figure legend, the reader is referred to the web version of this article.)

photocatalytic H_2 generation [59].

Based on the aforementioned experimental and theoretical results, the critical factors for the remarkable improvement on H_2 evolution performance should be the fast electron transfer behavior as well as efficient charge separation in the hetero-interface of CdS and CoP_x (Fig. 6c). Specifically, the CoP_x@CdS has been endowed with the capability to overcome undesired charge carrier recombination. Meanwhile, the interfacial engineering through Ca^{2+} dopant can promote the thermodynamic kinetics of H_2 production over the surface active sites on CoP_x. Owing to the interplay of CoP_x and Ca^{2+} dopant, the efficient interfacial charge transfer channel between CdS and CoP_x has been formed. Therefore, photogenerated electrons would transfer through the interlayer between CdS and CoP_x more efficiently under light illumination for enhancing H_2 generation.

4. Conclusions

In summary, PPh_3 has been successfully applied to fabricate carbon encapsulated ultrafine CoP_x nanoparticles on the surface of CdS. Meanwhile, Ca^{2+} as an alkaline earth metal ion may easily substitute the Cd^{2+} lattice sites of CdS, which has induced strong trap-state emission together with long-lived charge carriers. In-depth investigations on the transfer dynamics of photogenerated electron demonstrated fast charge transfer behavior in Ca-modified CoP_x@CdS, indicating the enhanced electron-hole separation ability than that of unmodified CdS. The surface Ca^{2+} may act as the interfacial mediator for accelerating the electron transfer from CdS to CoP_x for participate in the H_2 generation reaction. As the result, Ca-modified CoP_x@CdS can achieve 2441.5 μmol h^{-1} H_2 generation rate with an apparent quantum efficiency of 35.4% at 420 nm. Therefore, we hope this investigation would offer new opportunities and be beneficial for future modification on photocatalysts through metal dopants.

CRediT authorship contribution statement

Xiaohui Ren: Conceptualization, Data curation, Formal analysis, Methodology, Investigation, Writing – original draft. **Fei Liu:** Conceptualization, Investigation, Methodology, Validation. **Qi Wang:** Conceptualization, Validation. **Hui Song:** Investigation, Validation, Writing – review & editing. **Shunqin Luo:** Data curation, Validation, Writing – review & editing. **Sijie Li:** Validation. **Gaoliang Yang:** Visualization. **Bowen Deng:** Validation. **Zongyu Huang:** Software. **Xu-Sheng Wang:** Validation, Resources. **Li Shi:** Conceptualization, Methodology, Writing – review & editing. **Professor Jinhua Ye**: Supervision, Conceptualization, Writing – review & editing, Resources, Validation, Project administration, Funding acquisition.

Declaration of Competing Interest

The authors declare that they have no known competing financial interests or personal relationships that could have appeared to influence the work reported in this paper.

Acknowledgements

This work was supported by Japan Society for the Promotion of Science (JSPS) KAKENHI (JP18H02065), the World Premier International Research Center Initiative (WPI Initiative) on Materials Nanoarchitectonics (MANA), MEXT (Japan), Photoexcitonix Project in Hokkaido University, National Natural Science Foundation of China (Grant No. 21633004, 22001094, and 51872091), National Key R&D Program of China (Grant No. 2018YFC190503), the Fellowship of China Postdoctoral Science Foundation (2020M673057, 2020TQ0123), the International Program of Guangdong Provincial Outstanding Young Researcher, and the State Scholarship Fund by China Scholarship Council (CSC) (201808430219).

Appendix A. Supporting information

Supplementary data associated with this article can be found in the online version at doi:10.1016/j.apcatb.2021.120887.

References

[1] J.O. Abe, A.P.I. Popoola, E. Ajenifuja, O.M. Popoola, Hydrogen energy, economy and storage: review and recommendation, Int. J. Hydrog. Energy 44 (2019) 15072–15086, https://doi.org/10.1016/j.ijhydene.2019.04.068.
[2] C.J. Quarton, O. Tlili, L. Welder, C. Mansilla, H. Blanco, H. Heinrichs, J. Leaver, N. J. Samsatli, P. Lucchese, M. Robinius, S. Samsatli, The curious case of the conflicting roles of hydrogen in global energy scenarios, Sustain. Energy Fuels 4 (2020) 80–95, https://doi.org/10.1039/C9SE00833K.
[3] I. Staffell, D. Scamman, A. Velazquez Abad, P. Balcombe, P.E. Dodds, P. Ekins, N. Shah, K.R. Ward, The role of hydrogen and fuel cells in the global energy system, Energy Environ. Sci. 12 (2019) 463–491, https://doi.org/10.1039/C8EE01157E.
[4] H. Song, X. Meng, S. Wang, W. Zhou, X. Wang, T. Kako, J. Ye, Direct and selective photocatalytic oxidation of CH_4 to oxygenates with O_2 on cocatalysts/ZnO at room temperature in water, J. Am. Chem. Soc. 141 (2019) 20507–20515, https://doi.org/10.1021/jacs.9b11440.
[5] S. Luo, H. Lin, Q. Wang, X. Ren, D. Hernández-Pinilla, T. Nagao, Y. Xie, G. Yang, S. Li, H. Song, M. Oshikiri, J. Ye, Triggering water and methanol activation for solar-driven H_2 production: interplay of dual active sites over plasmonic ZnCu alloy, J. Am. Chem. Soc. 143 (2021) 12145–12153, https://doi.org/10.1021/jacs.1c04315.
[6] G. Liu, Y. Sheng, J.W. Ager, M. Kraft, R. Xu, Research advances towards large-scale solar hydrogen production from water, EnergyChem 1 (2019), 100014, https://doi.org/10.1016/j.enchem.2019.100014.
[7] X. Chen, S. Shen, L. Guo, S.S. Mao, Semiconductor-based photocatalytic hydrogen generation, Chem. Rev. 110 (2010) 6503–6570, https://doi.org/10.1021/cr1001645.
[8] C. Luo, X. Ren, Z. Dai, Y. Zhang, X. Qi, C. Pan, Present perspectives of advanced characterization techniques in TiO_2-based photocatalysts, ACS Appl. Mater. Interfaces 9 (2017) 23265–23286, https://doi.org/10.1021/acsami.7b00496.
[9] S. Luo, X. Ren, H. Lin, H. Song, J. Ye, Plasmonic photothermal catalysis for solar-to-fuel conversion: current status and prospects, Chem. Sci. 12 (2021) 5701–5719, https://doi.org/10.1039/D1SC00064K.
[10] H. Song, X. Meng, S. Wang, W. Zhou, S. Song, T. Kako, J. Ye, Selective photo-oxidation of methane to methanol with oxygen over dual-cocatalyst-modified titanium dioxide, ACS Catal. 10 (2020) 14318–14326, https://doi.org/10.1021/acscatal.0c04329.
[11] Z.-j Wang, H. Song, H. Liu, J. Ye, Coupling of solar energy and thermal energy for carbon dioxide reduction: status and prospects, Angew. Chem. Int. Ed. 59 (2020) 8016–8035, https://doi.org/10.1002/anie.201907443.
[12] J. Zeng, W. Zeng, H. Zeng, In situ plasmonic Au nanoparticle anchored nickel ferrite: an efficient plasmonic photocatalyst for fluorescein-sensitized hydrogen evolution under visible light irradiation, J. Solid State Chem. 253 (2017) 294–304, https://doi.org/10.1016/j.jssc.2017.06.005.
[13] G. Zeng, H. Zeng, L. Niu, J. Chen, T. Song, P. Zhang, Y. Wu, X. Xiao, Y. Zhang, S. Huang, A. Promising, Alternative for sustainable and highly efficient solar-driven deuterium evolution at room temperature by photocatalytic D_2O splitting, ChemSusChem 13 (2020) 2935–2939, https://doi.org/10.1002/cssc.202000562.
[14] J. Ran, J. Zhang, J. Yu, M. Jaroniec, S.Z. Qiao, Earth-abundant cocatalysts for semiconductor-based photocatalytic water splitting, Chem. Soc. Rev. 43 (2014) 7787–7812, https://doi.org/10.1039/C3CS60425J.
[15] H. Fei, J. Dong, M.J. Arellano-Jiménez, G. Ye, N.D. Kim, E.L.G. Samuel, Z. Peng, Z. Zhu, F. Qin, J. Bao, M.J. Yacaman, P.M. Ajayan, D. Chen, J.M. Tour, Atomic cobalt on nitrogen-doped graphene for hydrogen generation, Nat. Commun. 6 (2015) 8668, https://doi.org/10.1038/ncomms9668.
[16] S. Cao, Y. Chen, C.-C. Hou, X.-J. Lv, W.-F. Fu, Cobalt phosphide as a highly active non-precious metal cocatalyst for photocatalytic hydrogen production under visible light irradiation, J. Mater. Chem. A 3 (2015) 6096–6101, https://doi.org/10.1039/C4TA07149B.
[17] B. Tian, Z. Li, W. Zhen, G. Lu, Uniformly sized (112) facet Co_2P on graphene for highly effective photocatalytic hydrogen evolution, J. Phys. Chem. C 120 (2016) 6409–6415, https://doi.org/10.1021/acs.jpcc.6b00680.
[18] Z. Pan, Y. Zheng, F. Guo, P. Niu, X. Wang, Decorating CoP and Pt nanoparticles on graphitic carbon nitride nanosheets to promote overall water splitting by conjugated polymers, ChemSusChem 10 (2017) 87–90, https://doi.org/10.1002/cssc.201600850.
[19] X. Ren, D. Philo, Y. Li, L. Shi, K. Chang, J. Ye, Recent advances of low-dimensional phosphorus-based nanomaterials for solar-driven photocatalytic reactions, Coord. Chem. Rev. 424 (2020), 213516, https://doi.org/10.1016/j.ccr.2020.213516.
[20] X. Ren, L. Shi, Y. Li, S. Song, Q. Wang, S. Luo, L. Ren, H. Zhang, Y. Izumi, X. Peng, D. Philo, F. Ichihara, J. Ye, Single cobalt atom anchored black phosphorous nanosheets as an effective cocatalyst promotes photocatalysis, ChemCatChem 12 (2020) 3870–3879, https://doi.org/10.1002/cctc.202000546.
[21] J. Qin, H. Zeng, Photocatalysts fabricated by depositing plasmonic Ag nanoparticles on carbon quantum dots/graphitic carbon nitride for broad spectrum photocatalytic hydrogen generation, Appl. Catal. B 209 (2017) 161–173, https://doi.org/10.1016/j.apcatb.2017.03.005.
[22] H. Yang, Y. Zhang, F. Hu, Q. Wang, Urchin-like CoP nanocrystals as hydrogen evolution reaction and oxygen reduction reaction dual-electrocatalyst with

superior stability, Nano Lett. 15 (2015) 7616–7620, https://doi.org/10.1021/acs.nanolett.5b03446.
[23] J. Wang, P. Wang, C. Wang, Y. Ao, In-situ synthesis of well dispersed CoP nanoparticles modified CdS nanorods composite with boosted performance for photocatalytic hydrogen evolution, Int. J. Hydrog. Energy 43 (2018) 14934–14943, https://doi.org/10.1016/j.ijhydene.2018.06.101.
[24] P. Wang, T. Wu, Y. Ao, C. Wang, Fabrication of noble-metal-free CdS nanorods-carbon layer-cobalt phosphide multiple heterojunctions for efficient and robust photocatalyst hydrogen evolution under visible light irradiation, Renew. Energy 131 (2019) 180–186, https://doi.org/10.1016/j.renene.2018.07.028.
[25] Z. Sun, B. Lv, J. Li, M. Xiao, X. Wang, P. Du, Core–shell amorphous cobalt phosphide/cadmium sulfide semiconductor nanorods for exceptional photocatalytic hydrogen production under visible light, J. Mater. Chem. A 4 (2016) 1598–1602, https://doi.org/10.1039/C5TA07561K.
[26] X.-J. Wang, X. Tian, Y.-J. Sun, J.-Y. Zhu, F.-T. Li, H.-Y. Mu, J. Zhao, Enhanced Schottky effect of a 2D–2D CoP/g-C_3N_4 interface for boosting photocatalytic H_2 evolution, Nanoscale 10 (2018) 12315–12321, https://doi.org/10.1039/C8NR03846E.
[27] S. Cao, Y. Chen, H. Wang, J. Chen, X. Shi, H. Li, P. Cheng, X. Liu, M. Liu, L. Piao, Ultrasmall CoP nanoparticles as efficient cocatalysts for photocatalytic formic acid dehydrogenation, Joule 2 (2018) 549–557, https://doi.org/10.1016/j.joule.2018.01.007.
[28] J.-C. Wu, J. Zheng, P. Wu, R. Xu, Study of Native defects and transition-metal (Mn, Fe, Co, and Ni) Doping in a zinc-blende CdS photocatalyst by DFT and hybrid DFT calculations, J. Phys. Chem. C 115 (2011) 5675–5682, https://doi.org/10.1021/jp109567c.
[29] R. Shi, H.-F. Ye, F. Liang, Z. Wang, K. Li, Y. Weng, Z. Lin, W.-F. Fu, C.-M. Che, Y. Chen, Interstitial P-doped CdS with long-lived photogenerated electrons for photocatalytic water splitting without sacrificial agents, Adv. Mater. 30 (2018), 1705941, https://doi.org/10.1002/adma.201705941.
[30] H. Huang, B. Dai, W. Wang, C. Lu, J. Kou, Y. Ni, L. Wang, Z. Xu, Oriented built-in electric field introduced by surface gradient diffusion doping for enhanced photocatalytic H_2 evolution in CdS nanorods, Nano Lett. 17 (2017) 3803–3808, https://doi.org/10.1021/acs.nanolett.7b01147.
[31] H. Song, X. Meng, Z.-J. Wang, H. Liu, J. Ye, Solar-energy-mediated methane conversion, Joule 3 (2019) 1606–1636, https://doi.org/10.1016/j.joule.2019.06.023.
[32] J. Qin, J. Huo, P. Zhang, J. Zeng, T. Wang, H. Zeng, Improving the photocatalytic hydrogen production of Ag/g-C_3N_4 nanocomposites by dye-sensitization under visible light irradiation, Nanoscale 8 (2016) 2249–2259, https://doi.org/10.1039/C5NR06346A.
[33] K. Zhang, Z. Zhou, L. Guo, Alkaline earth metal as a novel dopant for chalcogenide solid solution: Improvement of photocatalytic efficiency of $Cd_{1-x}Zn_xS$ by barium surface doping, Int. J. Hydrog. Energy 36 (2011) 9469–9478, https://doi.org/10.1016/j.ijhydene.2011.05.058.
[34] M. Zhou, D. Han, X. Liu, C. Ma, H. Wang, Y. Tang, P. Huo, W. Shi, Y. Yan, J. Yang, Enhanced visible light photocatalytic activity of alkaline earth metal ions-doped CdSe/rGO photocatalysts synthesized by hydrothermal method, Appl. Catal. B 172–173 (2015) 174–184, https://doi.org/10.1016/j.apcatb.2015.01.004.
[35] S.L. Brock, S.C. Perera, K.L. Stamm, Chemical routes for production of transition-metal phosphides on the nanoscale: implications for advanced magnetic and catalytic materials, Chem. - Eur. J. 10 (2004) 3364–3371, https://doi.org/10.1002/chem.200305775.
[36] Y. Shi, B. Zhang, Recent advances in transition metal phosphide nanomaterials: synthesis and applications in hydrogen evolution reaction, Chem. Soc. Rev. 45 (2016) 1529–1541, https://doi.org/10.1039/C5CS00434A.
[37] S. Cao, C.-J. Wang, W.-F. Fu, Y. Chen, Metal phosphides as co-catalysts for photocatalytic and photoelectrocatalytic water splitting, ChemSusChem 10 (2017) 4306–4323, https://doi.org/10.1002/cssc.201701450.
[38] S.-S. Yi, J.-M. Yan, B.-R. Wulan, S.-J. Li, K.-H. Liu, Q. Jiang, Noble-metal-free cobalt phosphide modified carbon nitride: an efficient photocatalyst for hydrogen generation, Appl. Catal. B 200 (2017) 477–483, https://doi.org/10.1016/j.apcatb.2016.07.046.
[39] M.F. Saleem, H. Zhang, Y. Deng, D. Wang, Resonant Raman scattering in nanocrystalline thin CdS film, J. Raman Spectrosc. 48 (2017) 224–229, https://doi.org/10.1002/jrs.5002.
[40] Y. Hou, Y. Liu, R. Gao, Q. Li, H. Guo, A. Goswami, R. Zboril, M.B. Gawande, X. Zou, Ag@Co_xP core–shell heterogeneous nanoparticles as efficient oxygen evolution reaction catalysts, ACS Catal. 7 (2017) 7038–7042, https://doi.org/10.1021/acscatal.7b02341.
[41] G. Li, J. Yu, J. Jia, L. Yang, L. Zhao, W. Zhou, H. Liu, Cobalt–cobalt phosphide nanoparticles@nitrogen-phosphorus doped carbon/graphene derived from cobalt ions adsorbed saccharomycete yeasts as an efficient, stable, and large-current-density electrode for hydrogen evolution reactions, Adv. Funct. Mater. 28 (2018), 1801332, https://doi.org/10.1002/adfm.201801332.
[42] A.M. Elshahawy, C. Guan, X. Li, H. Zhang, Y. Hu, H. Wu, S.J. Pennycook, J. Wang, Sulfur-doped cobalt phosphide nanotube arrays for highly stable hybrid supercapacitor, Nano Energy 39 (2017) 162–171, https://doi.org/10.1016/j.nanoen.2017.06.042.
[43] J. Wang, Q. Yang, Z. Zhang, Selective synthesis of Magnetic Fe_2P/C and FeP/C core/shell nanocables, J. Phys. Chem. Lett. 1 (2010) 102–106, https://doi.org/10.1021/jz900075q.
[44] V. Ganeshchandra Prabhu, A.R. Paloly, N.G. Divya, M.J. Bushiri, Photocatalytic and ferromagnetic properties of electrically conducting multifunctional Ni/NiO nanocomposites in amorphous carbon matrix, Mater. Sci. Eng. 228 (2018) 132–141, https://doi.org/10.1016/j.mseb.2017.11.017.
[45] M.A. Tamor, W.C. Vassell, Raman "fingerprinting" of amorphous carbon films, J. Appl. Phys. 76 (1994) 3823–3830, https://doi.org/10.1063/1.357385.
[46] X. Ren, S. Wei, Q. Wang, L. Shi, X.-S. Wang, Y. Wei, G. Yang, D. Philo, F. Ichihara, J. Ye, Rational construction of dual cobalt active species encapsulated by ultrathin carbon matrix from MOF for boosting photocatalytic H_2 generation, Appl. Catal. B 286 (2021), 119924, https://doi.org/10.1016/j.apcatb.2021.119924.
[47] L.Z. Linganiso, G. Jacobs, K.G. Azzam, U.M. Graham, B.H. Davis, D.C. Cronauer, A. J. Kropf, C.L. Marshall, Low-temperature water–gas shift: strategy to lower Pt loading by doping ceria with Ca^{2+} improves formate mobility/WGS rate by increasing surface O-mobility, Appl. Catal. A 394 (2011) 105–116, https://doi.org/10.1016/j.apcata.2010.12.043.
[48] Q. An, X. Meng, P. Sun, High-performance fully nanostructured photodetector with single-crystalline CdS nanotubes as active layer and very long ag nanowires as transparent electrodes, ACS Appl. Mater. Interfaces 7 (2015) 22941–22952, https://doi.org/10.1021/acsami.5b06166.
[49] S. Yılmaz, İ. Polat, M. Tomakin, E. Bacaksız, Transparent and conductive CdS:Ca thin films for optoelectronic applications, Appl. Phys. A 126 (2020) 555, https://doi.org/10.1007/s00339-020-03752-7.
[50] W. Guo, Z. Liang, J. Zhao, B. Zhu, K. Cai, R. Zou, Q. Xu, Hierarchical COBALT PHOSPHIDE HOLLOW NANOCAGES TOWARD ELECTROCATALYTIC AMMONIA SYNTHESIS UNDER AMBIENT PRESSURE AND ROOM TEmperature, Small Methods 2 (2018), 1800204, https://doi.org/10.1002/smtd.201800204.
[51] Q. Liang, F. Shi, X. Xiao, X. Wu, K. Huang, S. Feng, Insitu growth of CoP nanoparticles anchored on black phosphorus nanosheets for enhanced photocatalytic hydrogen production, ChemCatChem 10 (2018) 2179–2183, https://doi.org/10.1002/cctc.201701907.
[52] T. Leijtens, G.E. Eperon, A.J. Barker, G. Grancini, W. Zhang, J.M. Ball, A.R. S. Kandada, H.J. Snaith, A. Petrozza, Carrier trapping and recombination: the role of defect physics in enhancing the open circuit voltage of metal halide perovskite solar cells, Energy Environ. Sci. 9 (2016) 3472–3481, https://doi.org/10.1039/C6EE01729K.
[53] Z. Sun, H. Zheng, J. Li, P. Du, Extraordinarily efficient photocatalytic hydrogen evolution in water using semiconductor nanorods integrated with crystalline Ni_2P cocatalysts, Energy Environ. Sci. 8 (2015) 2668–2676, https://doi.org/10.1039/C5EE01310K.
[54] H. Zhang, Z. Ma, J. Duan, H. Liu, G. Liu, T. Wang, K. Chang, M. Li, L. Shi, X. Meng, K. Wu, J. Ye, Active sites implanted carbon cages in core–shell architecture: highly active and durable electrocatalyst for hydrogen evolution reaction, ACS Nano 10 (2016) 684–694, https://doi.org/10.1021/acsnano.5b05728.
[55] G. Zhao, Y. Sun, W. Zhou, X. Wang, K. Chang, G. Liu, H. Liu, T. Kako, J. Ye, Superior photocatalytic H_2 production with cocatalytic Co/Ni species anchored on sulfide semiconductor, Adv. Mater. 29 (2017), 1703258, https://doi.org/10.1002/adma.201703258.
[56] L. Tong, L. Ren, A. Fu, D. Wang, L. Liu, J. Ye, Copper nanoparticles selectively encapsulated in an ultrathin carbon cage loaded on $SrTiO_3$ as stable photocatalysts for visible-light H_2 evolution via water splitting, Chem. Commun. 55 (2019) 12900–12903, https://doi.org/10.1039/C9CC05228C.
[57] I. Fernández, N. Holzmann, G. Frenking, The valence orbitals of the alkaline-earth atoms, Chem. - Eur. J. 26 (2020) 14194–14210, https://doi.org/10.1002/chem.202002986.
[58] B. Rösch, T.X. Gentner, J. Langer, C. Färber, J. Eyselein, L. Zhao, C. Ding, G. Frenking, S. Harder, Dinitrogen complexation and reduction at low-valent calcium, Science 371 (2021) 1125–1128, https://doi.org/10.1126/science.abf2374.
[59] I. Majeed, M.A. Nadeem, M. Al-Oufi, M.A. Nadeem, G.I.N. Waterhouse, A. Badshah, J.B. Metson, H. Idriss, On the role of metal particle size and surface coverage for photo-catalytic hydrogen production: a case study of the Au/CdS system, Appl. Catal. B 182 (2016) 266–276, https://doi.org/10.1016/j.apcatb.2015.09.039.